

Modelling of Shear-critical, Lightly Reinforced Concrete T-beams with Externally Bonded CFRP using ATENA Science

Njoko, F.H.¹, Tambusay, A.^{1*}, Jamieson, A.², Suryanto, B.², and Suprobo, P.¹

Abstract: This paper presents the finite element modelling of shear-critical reinforced concrete beams strengthened with U-wrapped CFRP fabrics using ATENA. Fracture-plastic constitutive models, implemented in the context of smeared crack and crush-band approach, were employed to represent the nonlinear behaviours of concrete. CFRP U-wraps were modelled as smeared reinforcement and bonded to the concrete surface using an interface element, considering appropriate bond properties. To this end, two large lightly reinforced concrete T-beams from tests undertaken by Brindley in 2018 were analysed and predictions of the load-deflection response and failure mode are presented to demonstrate the accuracy of the modelling. Moreover, parametric analyses were performed to assess the effectiveness of CFRP U-wraps for strengthening deteriorated members. It is shown that the response of the beams can be predicted accurately, capturing successfully the brittle shear failure mode observed experimentally. It is also shown that CFRP U-wraps are useful for reducing the brittleness of shear-critical beams.

Keywords: Finite element modelling; CFRP; shear; strengthening; T-beams; U-wrap.

Introduction

The performance of reinforced concrete members generally decreases with time due to ageing, deterioration of the concrete and reinforcing steel, and damage caused by external loads. This is commonly reflected in a gradual reduction in load-carrying capacity and stiffness with time. As damage progresses with time, distressed reinforced concrete members would therefore give early considerable warning prior to failure, in the form of, for example, large crack formations or excessive deflection. However, this may not be the case for old structural members in historic structures, which are lightly reinforced and have their shear capacities compromised by ongoing deterioration processes. Such members may fail without prior warning, and possibly result in loss of life. Under such circumstances, engineers often resort to available repair and strengthening techniques and one of the emerging methods that has gained increasing popularity is fibre reinforced polymer (FRP) due to its high strength-to-weight ratio, corrosion resistance, and ease of installation on site [1,2].

Various methods of FRP installation have now been developed, including direct wrapping around a structural member [3], near surface mounting [4], deep embedment method [5] and U-wrapping [6]. This paper focuses on the latter as it is considered as the most utilised method for beam applications due to its ease of implementation in practice. U-wrapping generally involves bonding FRP sheets and resin fabrics to the side and bottom surfaces of a concrete beam, and the effectiveness of this strengthening technique has been found to rely primarily on their bonding to the concrete surface [7]. Careful consideration should therefore be given to designing FRP with adequate development length that would prevent premature debonding. Other important factors include the orientation and thickness of the FRP, the type of FRP and resin used, and loading and exposure conditions.

Despite the growing number of resin-bonded FRP applications in the past few decades, there is still a lack of understanding as to how deteriorated reinforced concrete members strengthened with FRP would behave under loading. More specifically, there is limited knowledge of the shear-critical response of FRP strengthened members due to the complexity involved, in particular the challenge to assess if there is a risk of failure under service loads. The advances in nonlinear analysis of reinforced concrete structures, particularly on the modelling front [8-10], and the exponential growth in computing power can make an important contribution in this regard. Advanced numerical modelling can provide engineers with a powerful tool which can be used for the assessment of the safety and integrity of distressed structures [11] and the behaviour expected after retrofitting. It can

¹ Department of Civil Engineering, Faculty of Civil, Planning and Geo Engineering, Sepuluh Nopember Institute of Technology, Surabaya, East Java 60111, INDONESIA.

² School of Energy, Geoscience, Infrastructure and Society, Institute for Sustainable Built Environment, Heriot-Watt University, Edinburgh EH14 4AS, Scotland, UNITED KINGDOM.

*Corresponding author; Email: asdam@its.ac.id

Note: Discussion is expected before November, 1st 2023, and will be published in the "Civil Engineering Dimension", volume 26, number 1, March 2024.

Received 01 June 2023; revised 15 July 2023; accepted 17 July 2023.

also be of value for exploring various repair and strengthening strategies with relatively minimum resources to laboratory and/or site testing [12].

In this paper, use is made of a nonlinear finite element analysis software ATENA Science [13]. Emphasis is placed on the user-defined constitutive models in the software and in the modelling procedures which can be used to account for debonding in shear-deficient reinforced concrete members. The accuracy of the modelling is demonstrated through a simulation of shear-critical reinforced concrete T-beams with and without FRP strengthening.

Overview of Brindley T-beams

The T-beam test series referred to in this study was taken from the experiments undertaken by Brindley at the University of Bath in 2018 [14]. Ten T-beams of two different sizes were tested in total but only two beams were selected and analysed in this paper. This includes the large control beam with no CFRP fabrics (denoted LBC) and one of the large beams strengthened with externally bonded CFRP fabrics, in the form of a U-wrap configuration (denoted LB1U). Number 1 here refers to the low reinforcement ratio of CFRP used in the beams (e.g., 0.7%), following the notation used in the original experiment.

The schematic diagrams of the geometry, cross-section details and reinforcement layouts for the two beams are displayed in Figure 1, with pertinent details summarised in Table 1. The beams were 0.72m

deep, 0.76m/0.3m wide (flange/web) and 4.5m long. It was simply supported with a span of 4.2 m, and subjected to a point load at midspan, giving a shear span-to-depth ratio of 3.5. To prevent the yielding of the longitudinal reinforcement, the beams were reinforced with six H32 bottom longitudinal bars (arranged in two layers; H referring to high strength steel of grade B500C [15] and 32 denoting the bar diameter), corresponding to a reinforcement ratio of 2.2%. Each bar was extended past the supports and bent up at its ends to provide adequate anchorage. To promote shear failure, transverse reinforcement in the test span was provided in the form of closed links of 8mm diameter plain (mild steel) bar at 360mm spacing (or 0.6d, corresponding to a reinforcement ratio of 0.1%). Within the other half of the span, H12 closed links were provided at 150mm spacing.

Beam LB1U had the same geometry and reinforcing details as Beam LBC, but with the addition of two layers of 0.5mm-thick CFRP fabrics (modulus elasticity of 85GPa and ultimate tensile strength 903MPa) externally bonded to the side and bottom surfaces of the web of the beam in a U-wrap configuration (see Figure 2). A summary of the reinforcement properties used in the experiment is provided in Table 2.

Table 2. Material Properties of Reinforcing Bar

Diameter (mm)	f_y (MPa)	f_u (MPa)
8	336	438
12	518	586
16	538	631
32	510	587

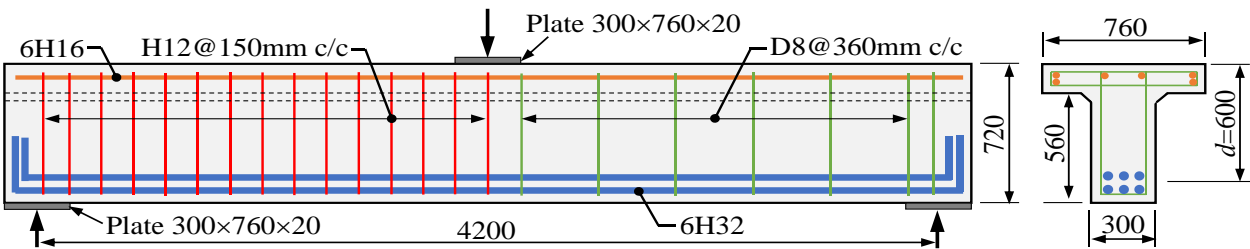


Figure 1. Elevation and Cross-section Details of Brindley T-beams

Table 1. Cross-section, CFRP and Reinforcement Details.

Beam	Conc.	CFRP			Reinforcement			Test Span	Non-test Span
	f_{cu} (MPa)	ρ_f (%)	t_f (mm)	ρ_l (%)	Top Bar	Bottom Bar	ρ_v (%)		
LBC	55	–	–	2.2	6H16	6H32	0.1	2D8@360	2H12@150
LB1U	60	0.7	0.5+0.5	2.2	6H16	6H32	0.1	2D8@360	2H12@150



Figure 2. Layout of CFRP Strengthening for Beam LB1U

ATENA Modelling

The two beams were simulated in a 3D nonlinear finite element (FE) analysis software ATENA Science 5.9, developed by Cervenka Consulting [13]. It consists of two main integrated software packages: GiD and ATENA Studio. GiD is a graphic-based pre-processor and can be used to create a FE model and generate input data such as material properties for concrete and steel, boundary conditions and mesh generation. ATENA Studio serves two functions in ATENA Science: a solver and a post-processor. When a FE model is run in GiD, it transfers the generated FE mesh and associated input data to ATENA Studio, which then performs calculations (hence solver) and displays the computed results during an analysis (e.g., load-deflection response, deformed shapes, stress/strain distributions, and crack patterns [11,13]). This real-time visualisation is a unique feature of ATENA Studio which is rarely available in other FE packages. Once the analysis is complete, the computed results at different analysis steps can be viewed for interpretation and further analysis (hence post-processor).

Constitutive Models

In ATENA, the nonlinear behaviour of concrete is represented using a fracture-plastic constitutive model [8,11-13] to account for damage to the concrete resulting from cracking and crushing. This model is implemented within the small strain assumption and the decomposition of strains into elastic, plastic, and fracturing components. Each of these strain components is used to compute stresses in the concrete using the constitutive relations described below.

Figures 3(a)-(c) display graphical representations of the constitutive models employed in this study [11-13]. As illustrated in this Figure, the Menétrey-William plasticity model [16] is used to model the behaviour of concrete in compression. In this model, a failure surface employing a set of hardening/softening parameters is used to simulate the process of concrete crushing. As compressive stress increases beyond the elastic limit (hence hardening), the stress σ_c to the peak strength is related to the equivalent plastic strain ε_{eqp} using an elliptical equation [11-13]:

$$\frac{\sigma_c}{f_c} = f_{c0} + (f_c - f_{c0}) \sqrt{1 - \left(\frac{\varepsilon_{cp} - \varepsilon_{eqp}}{\varepsilon_{cp}}\right)^2} \quad (1)$$

where f_c is the compressive strength of concrete (MPa); f_{c0} is the compressive stress that corresponds to the onset of plasticity (taken as twice the concrete tensile strength) (MPa); and ε_{cp} is the plastic strain that corresponds to the compressive strength (onset of softening) ($= f_c/E_c$). The initial modulus of elasticity of the concrete E_c is

$$E_c = (6000 - 15.5f_{cu})\sqrt{f_{cu}} \quad (2)$$

where f_{cu} is the cube compressive strength of concrete ($= f_c / 0.85$).

The post-peak (softening) response of concrete in compression is calculated based on the computed compressive displacement w_c . Although an accurate post-peak model has been developed [8], a rather simple model is used here based on the assumption that the compressive stress beyond the peak decreases linearly to zero stress at a prescribed displacement w_d . Furthermore, to deal with mesh size dependency, the compressive displacement w_c is related to the plastic strain at the compressive strength ε_{cp} and the crush band size L_c , as given by

$$w_c = (\varepsilon_{eqp} - \varepsilon_{cp})L_c \quad (3)$$

The minimum crack band size is determined in accordance with the smallest dimension of the structural geometry in the section of interest [9]. In this work, the width of the beam was used as the minimum crush band size.

The tensile (fracture) model implements the Rankine failure criterion. In essence, this model comprises three main planes that form a tetrahedron in a 3D stress space (see Figure 3(b)). Embedded within the formulation of fracture analysis is the post-cracking (softening) response of concrete which, in this work, is represented by an exponential softening function [9,11]. It relates to the tensile stress of concrete σ_t to the crack opening displacement w using the empirical model proposed by Hordijk [17]:

$$\frac{\sigma_t}{f_t} = \left(1 + \left(c_1 \frac{w}{w_{cr}}\right)^3\right) e^{-c_2 \frac{w}{w_{cr}}} - \frac{w}{w_{cr}} (1 + c_1^3) e^{-c_2} \quad (4)$$

where f_t is the concrete tensile strength ($= 0.24f_{cu}^{\frac{2}{3}}$); w_{cr} is the crack opening at the complete release of stress ($= 5.14 \frac{G_f}{f_t}$) with G_f being the fracture energy of concrete ($= G_{f0} \left(\frac{f'_t}{10}\right)^{0.7}$) and G_{f0} being the basic value of fracture energy (N/m), which is related to the maximum aggregate size; and c_1 and c_2 are empirical constants (taken as 3 and 6.93 respectively) [11-13,18,19]. To deal with mesh size dependency, the crack opening displacement w is related to the tensile strain ε_t through the crack band size L_t , as given by

$$w = \varepsilon_t L_t \quad (5)$$

The crack band size is calculated for each element from the projection of the element length to the plane perpendicular to the crack direction.

At the onset of cracking, the above models are employed in the local crack coordinate system, following the crack directions in the concrete (at present, a

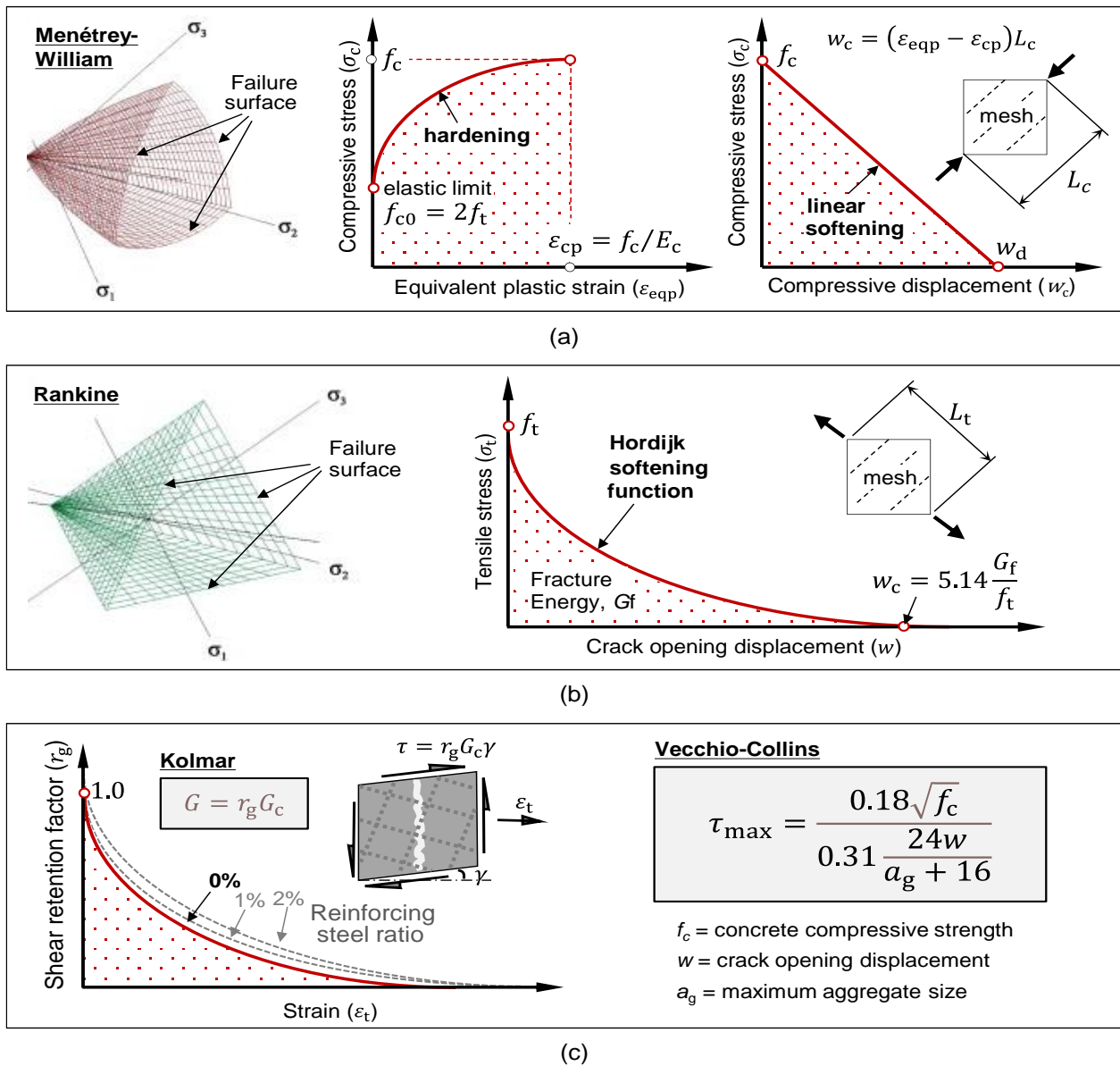


Figure 3. Constitutive Models for Concrete: (a) Compression; (b) Tension; and (c) Shear-transfer [11-13]

maximum of three orthogonal cracks can be considered). Three crack models are available in ATENA: rotating crack model, fixed crack model, and a combination of the two (hybrid crack model). In rotating crack models, crack directions in an element are allowed to rotate and follow the current principal strain directions in the concrete. This assumption allows cracked concrete to be treated as an orthotropic material (i.e., the use of compression and tension constitutive models is needed). Conversely, with fixed crack models, crack directions remain fixed regardless of the rotation of the principal strain directions in the concrete. When the principal strains no longer align with the crack directions, this will result in crack movement along crack surfaces (i.e., crack slip) and the development of shear stresses across the cracks. For this reason, the additional use of shear transfer model is required. In this work, the fixed crack model

was used as it provides a better representation of the physical behaviour of a real crack.

The shear transfer model adopted in this work requires the determination of two aspects: shear stiffness and shear strength. As illustrated in Figure 3(c), the shear stiffness after cracking G is related to the initial shear stiffness G_c through a shear retention factor r_g , following the model proposed by Kolmar [20]:

$$G = r_g G_c \quad (6)$$

$$r_g = c_3 \frac{-\ln\left(\frac{1000\varepsilon_t}{c_1}\right)}{c_2} \quad (7)$$

where the strain ε_t is normal to the crack direction; c_1 and c_2 are constant parameters which are dependent on the amount of steel reinforcement crossing a crack

(taken conservatively as 5.34 and 10.84, respectively, as used for plain concrete); and c_3 is a user scaling factor (taken as 1.0). Regarding the shear strength, the maximum shear stress that can be transmitted across a crack τ_{max} is assumed to follow the model proposed by Vecchio and Collins [21]:

$$\tau_{max} = \frac{0.18\sqrt{f_c}}{0.31\frac{24w}{a_g+16}} \quad (8)$$

where w is the crack opening displacement (mm) and a_g is the maximum aggregate size (mm). For more detailed information, readers are referred to [11-13].

In ATENA, reinforcement can be modelled as either a discrete or a smeared representation. In a discrete representation, the modelling of each individual bar is required, generally using a 1D truss element (only axial stiffness is considered). The smeared representation is more straightforward as steel bars are assumed to be distributed over the entire volume of an element. As a result, only the ratio of the total area of reinforcement (along any direction) to the area of the element needs to be defined. In this work, the discrete method was used for the reinforcing bars while the smeared representation was used for the CFRP fabrics. Reinforcement stresses are related to strains using a multi-linear stress-strain relation (see Figure 4). A linear stress-strain relation was used for the CFRP. The stress value upon failure is reduced to 1% of its tensile strength (instead of 0) to allow for stress redistribution upon failure.

FRP Modelling

In ATENA, two general modelling strategies can be employed to model FRP fabric in a smeared manner [1,22,23]:

- (i) 2D membrane elements employing plasticity/composite material; and
- (ii) 3D shell elements employing plasticity/composite material.

Membrane is a 2D element and hence can only take into consideration in-plane stiffnesses, whereas a 3D shell element can consider both in-plane and out-of-

plane stiffnesses. In this study, the use of membrane elements is considered adequate due to small thickness of the CFRP fabrics used in the beam, in comparison with the overall beam thickness. Regarding the input material, in the plasticity approach, FRP fabric and epoxy resin can only be treated as a single isotropic material. On the contrary, the composite method allows the two materials, with their own unique properties, to be explicitly considered. Using this approach, the FRP can also be treated as an orthotropic material. In this study, the properties used for epoxy resin to represent the bonding interface are provided in Table 3.

Table 3. Material Properties of Epoxy Resin (adapted from [24]).

Parameter Input	Interface Value	Unit
Tangential Stiffness, K_{TT}	70000	MN/m ³
Normal Stiffness, K_{NN}	260000	MN/m ³
Tensile Strength, f_t	2.7	MPa
Cohesion, c	4.8	MPa

To allow for the bond between the epoxy and concrete substrate to be considered, the surface contact between the two materials needs to be explicitly modelled. There are three modelling strategies:

- (i) Perfect bond [23,25,26]. In this case, bond failure is assumed to occur on concrete substrate beneath the epoxy resin. The use of fine mesh was recommended to allow for the cracking of concrete to be captured accurately [29];
- (ii) One-dimensional nonlinear spring placed between concrete and resin with the spring properties derived from the relationship between the interfacial shear stress and slip values; and
- (iii) Three-dimensional interface element with zero thickness between concrete and resin [1,23,27-31]. In this case, the interface parameters need to be defined and derived from the experimental data or theoretical models based on linear or nonlinear fracture mechanics [22,24,32-34].

In this work, option (iii) was adopted to allow for complex interactions between FRP and concrete substrate to be fully captured including the presence of transverse/confining pressure.

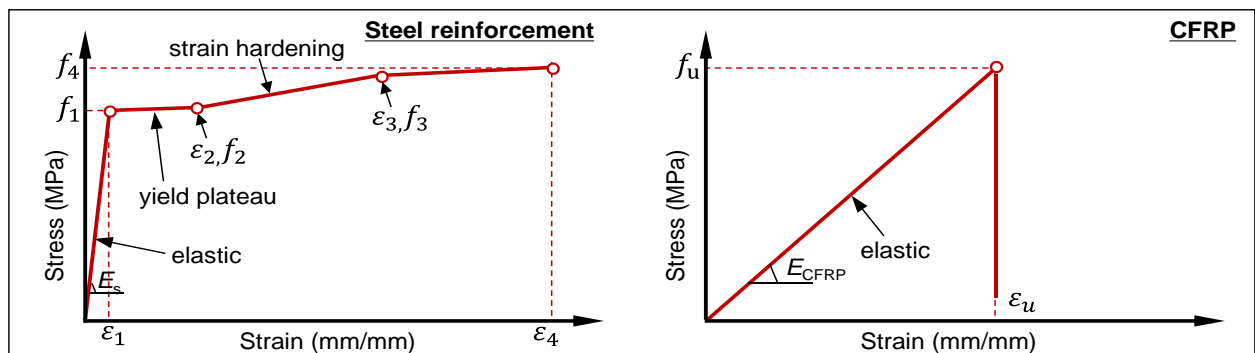


Figure 4. Constitutive Models for Reinforcement and CFRP

Finite Element Model

Figure 5(a) displays the finite element mesh and boundary conditions created for Beam LBC. Three types of elements were used: (i) linear hexahedral elements with a uniform mesh size of 40 mm for representing the concrete beam; (ii) linear tetrahedral elements for modelling the steel plates; and (iii) linear truss elements for representing the reinforcing bars. A bond-slip relation was considered for the plain bars (i.e., the shear links in the test span), whereas for all other bars, the bond between concrete and reinforcement was assumed to be in perfect condition (e.g., no bond-slip consideration). For Beam LB1U, the U-wrap and resin were represented by 2D membrane elements (essentially as reinforced resin), whereas the interfacial bond was represented by zero-thickness interface elements; these elements were bonded to the concrete surface via an auxiliary surface (see

Figure 5(b)). In both models, a point load was applied at the centre of the upper surface of the loading plate at midspan as an increasing displacement of 0.4 mm per step. Three monitoring points were considered: one placed underside the beam at midspan to measure the beam deflection and two others placed at the bottom supports to measure support reactions.

Results and Discussion

Figure 6(a) compares the predicted and observed load-deflection responses of the beams, along with the corresponding crack patterns and maximum principal strains at four stages of loading in Figures 6(b) and (c). In general, the response of these two beams can be characterised as shear in nature, as indicated by the formation of a localised diagonal crack in one of the shear spans (attributed mainly to the inadequate amount of shear links provided).

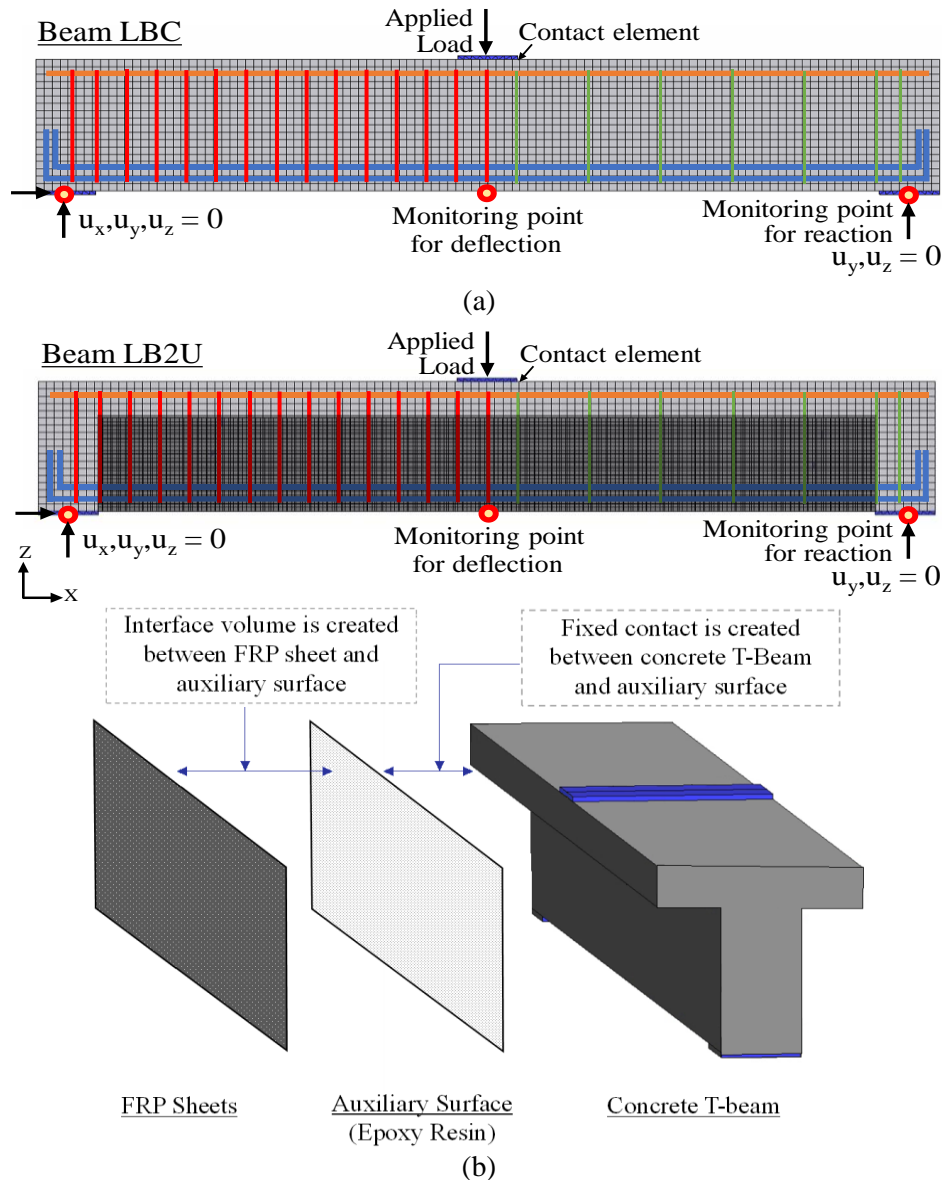


Figure 5. Finite Element Meshes used in the Analysis: (a) LBC and (b) LB1U

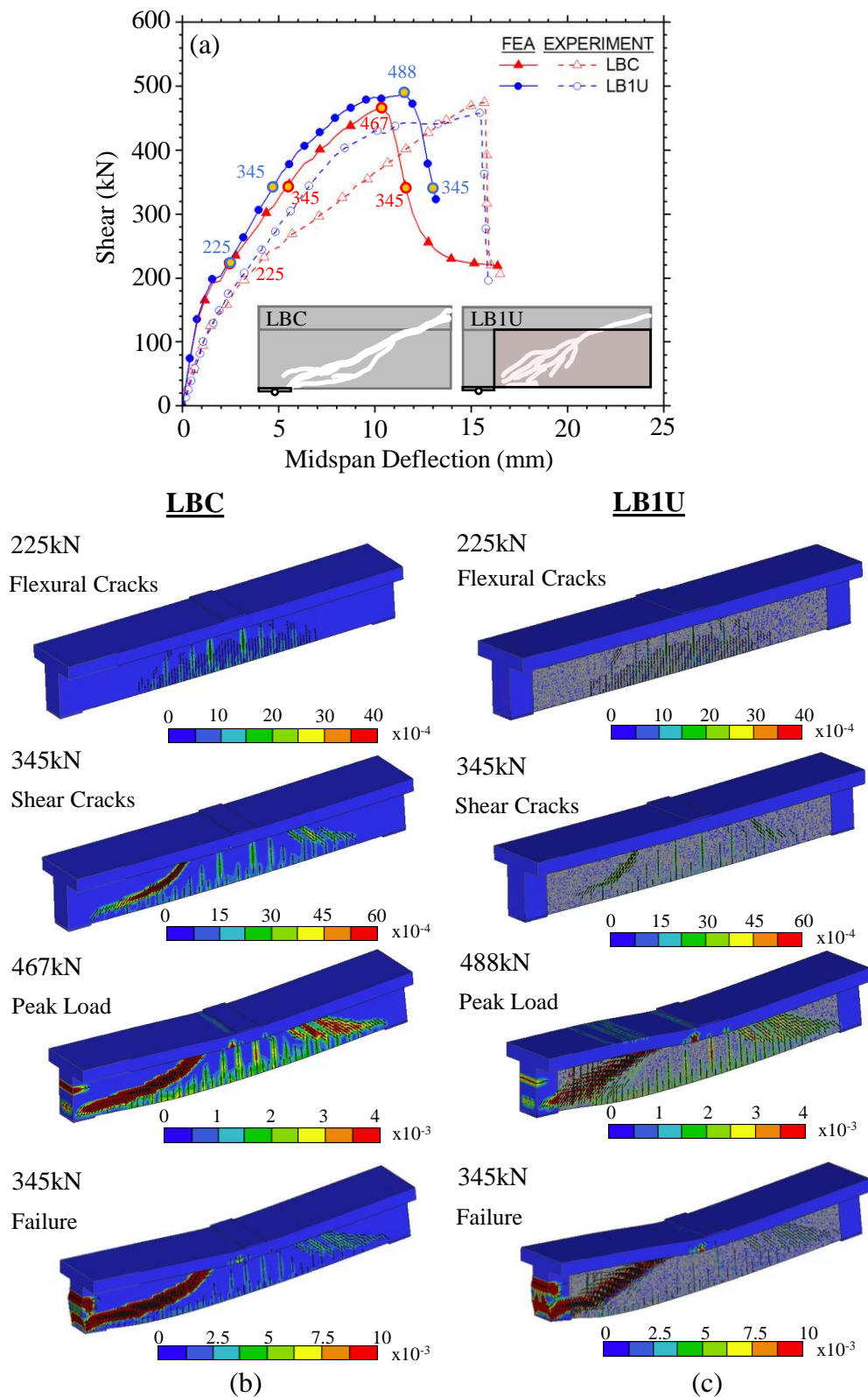


Figure 6. Responses of Large Beams: (a) Shear-deflection Relationships; (b)-(c) Crack Patterns and Maximum Principal Strains of LBC and LB1U

With reference to Figure 6(a), it is apparent that there is a reasonable agreement between the predicted and observed responses. A notable discrepancy is noted for Beam LB1U in which the prediction overestimates the beam-shear capacity. This might be partly

attributed to a more significant (and localised) development of shear crack in the web region of the test specimen, which triggers premature debonding, as reported in the experiment [14]. This is reflected by the lower post-cracking stiffnesses that are observed

from the experiment. The observed initial stiffnesses are also notably lower than the predictions, which might be attributed to the result of drying-induced shrinkage cracking which is not accounted for in the analysis.

Parametric Study

In this section, the results of a parametric study investigating the influence of commonly encountered deterioration in real-world conditions are presented. The parameters studied include:

- (i) Load sequence (LS). To simulate a real-life situation, the beam was loaded to 50% of its nominal capacity, subsequently strengthened with CFRP fabrics and then reloaded to failure.
- (ii) Reduction in bond properties (BR). In this case, the tensile strength and cohesion were reduced to 10% of their initial values. It is worth mentioning that the analysis, in this case, was done as (i), where the CFRP with reduced bond properties was activated after pre-loading.
- (iii) Reduction in transverse reinforcement (S-FR). In this case, the shear links in the test span were completely removed to represent extensive deterioration and full debonding of these bars. The CFRP was activated after the bar reductions and preloading to 50% of the capacity of Beam LBC.
- (iv) Reduction in longitudinal bars. The first run involved a cross-sectional reduction of the first (bottom) layer of tension bars by half (F-HR), while the second run considered a complete removal of this layer (F-FR). In both cases, the bottom part of the shear link was removed. This was to simulate severe corrosion and full debonding of longitudinal bars closest to the surface. The CFRP was activated as per (iii).
- (v) Reduction in both longitudinal and transverse reinforcements (SF-HR). In this case, the first (bottom) layer of the tension bars and shear links in the test span were reduced by half to further simulate extensive deterioration due to corrosion. As before, the CFRP was activated as per (iii).
- (vi) Variation of CFRP fabrics. Two additional types of FRP (SIKA CFRP and PET FRP) are studied to further explore their effectiveness in dealing with shear strengthening. The properties of these FRP are presented in Table 4.

Table 4. Material Properties of CFRP Fabrics

Parameter Input	TYFO	SIKA	PET	Unit
Tensile Strength, f_t	903	4,300	719	MPa
Modulus of Elasticity, E	85,000	238,000	9,350	MPa
Ultimate Strain, ε_u	0.9	1.8	6.7	%
Thickness, t_f	0.5	0.131	0.841	mm

Figures 7(a)-(f) display the shear-deflection responses and final crack patterns of the simulated beams, with

each beam labelled according to the parameters considered in (i)-(vi) above. In these figures, the predicted shear-deflection responses of Beams LBC and LB1U are also added for comparative purposes. Inspection from Figure 7(a) reveals that the U-wraps provide adequate strengthening, albeit displaying slightly lower shear and deflection capacities. Beam LS displays similar failure crack patterns to Beam LB1U, with final failure triggered by interface debonding. However, as the U-wraps in Beam LS were activated at a later stage (i.e., after preloading to 50% of its capacity), this beam displays a more localised band of diagonal cracking, which triggers debonding (and hence failure) at lower stresses. A similar response is also noted from the response of Beam BR shown in Figure 7(b) where the 90% reduction in bond strength is considered. However, this further reduction in bond properties does not appear to affect the strengthening performance of the U-wraps much, probably due to the dominant influence of the major diagonal shear crack as a result of the debonding of plain bars in the web region.

In contrast to the first two cases, the shear capacity of Beam S-FR is 13% lower than Beam LBC, due to the absence of shear links in the test span (see Figure 7(c)). However, it is interesting to note that, due to the presence of U-wraps, Beam S-FR displays a slightly higher post-cracking stiffness and eventually fails in a less brittle manner than Beam LBC, as indicated by the relatively constant load after the peak before eventually dropping off as a result of shear failure. The latter can be associated with the distributed nature of the cracks in the web region of Beam S-FR when compared to Beam LBC. This clearly indicates the usefulness of U-wraps in reducing brittleness and in enhancing post-peak ductility.

With reference to Figure 7(d), it is evident that the reduction in the amount of tension reinforcement is shown to lower the post-cracking stiffness and shear capacity of Beams F-HR and F-FR, with a reduction in a shear capacity of 11% and 17% respectively. However, it is worth noting that based on the amount of longitudinal and transverse reinforcement considered, the U-wrap is found useful to distribute cracks in the web region of the beam and promote a shift in the failure mode toward flexure (in this case, from shear dominant to shear-flexure). The post-peak ductility is also improved. A similar trend is evident in Figure 7(e).

Considering the influence of CFRP types (e.g., TYFO (used in the original experiment), SIKA and PET), it is apparent from Figure 7(f) that all beams exhibit similar initial and post-cracking stiffnesses, regardless of the type of CFRP used. However, it is interesting to note that the use of PET-wrap results

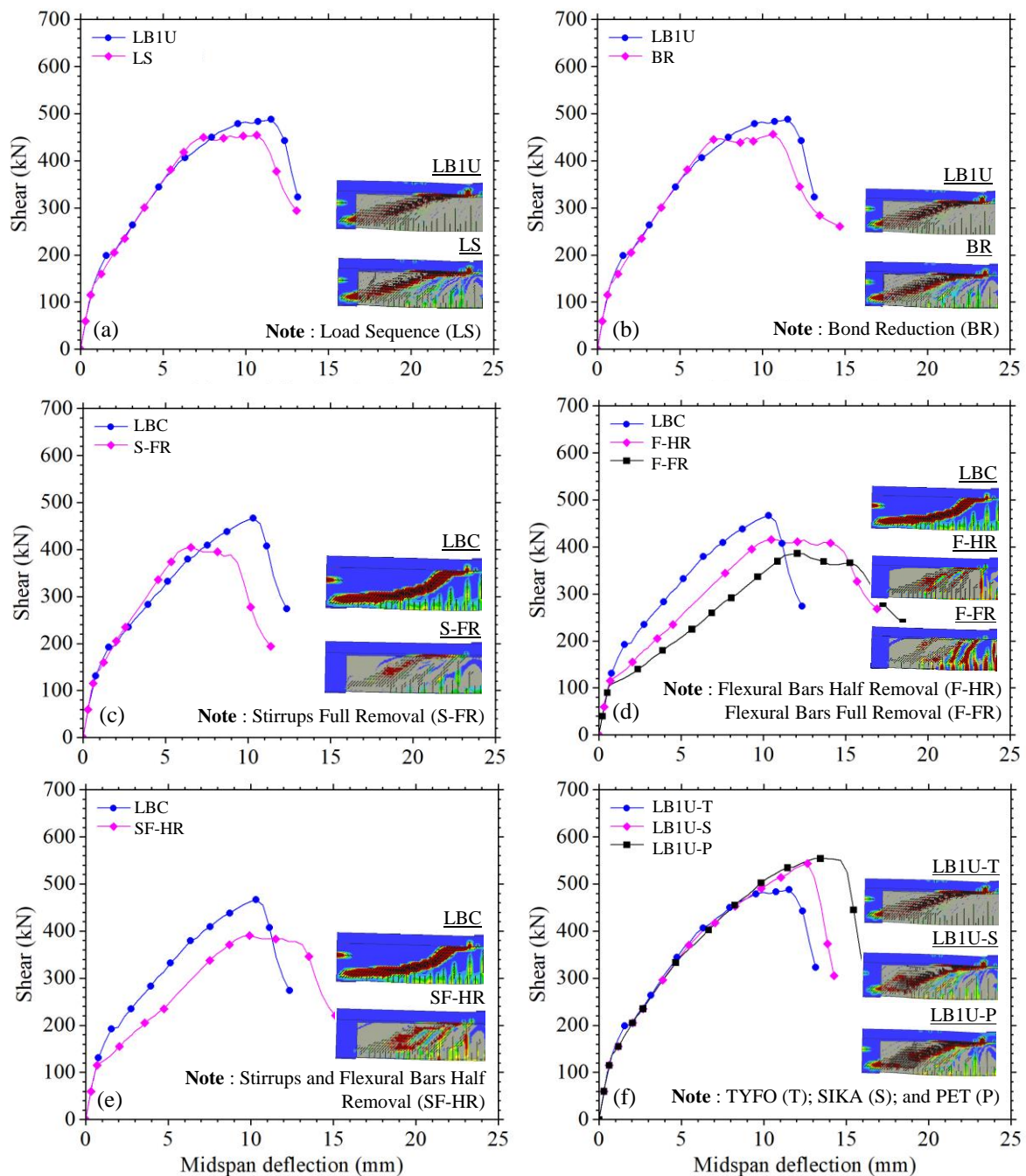


Figure 7. Shear-deflection Responses from Parametric Analyses. Effects of (a) Load Sequence and Reductions in (b) Bond Properties; (c) Transverse Reinforcement; (d) Longitudinal Reinforcement; and (e) Longitudinal and Transverse Reinforcement. (f) Effects of FRP Materials

in the highest predicted load and deflection capacities than the other two materials despite its lowest tensile strength. This might be related to its high tensile strain property and relatively low stiffness ($=7.9\text{kN/mm}$). The combined effects of which might be beneficial in reducing the extent of debonding in the vicinity of the localised shear cracks. Regarding the use of SIKA-wrap, an increase in the load and deflection capacities by $\sim 10\%$ is evidently predicted despite being the thinnest material among the three.

Concluding Remarks

The work presented highlights the application of a nonlinear finite element analysis program ATENA in the study of shear-critical, lightly reinforced concrete T-beams with u-wrapped CFRP strengthening. Additionally, detailed parametric analyses were performed to simulate the effects of commonly reported deterioration in reinforced concrete beams. Based on the work presented above, the following conclusions can be drawn:

1. Nonlinear finite element procedures incorporated in ATENA, along with the use of user-defined fracture-plastic constitutive models of concrete presented in this article, are shown to provide accurate predictions of the shear-critical reinforced concrete beams with and without CFRP strengthening. A reasonable agreement in predicted and observed responses was obtained.
2. Accurate predictions of failure modes were obtained. The failure of the beam with no strengthening was preceded by the formation of diagonal tension cracks, which triggered a brittle failure with a considerable drop in load after reaching its peak. Failure of a geometrically similar beam strengthened with CFRP U-Wraps was due to interface debonding, which is consistent with the experimental finding.
3. Activating CFRP after preloading (e.g., 50% of its nominal capacity) was found to yield a slightly lower shear capacity (about 7%) than the case when the CFRP was activated from the beginning of the analysis. However, reductions in the bond interface were found to have no significant effect on the shear capacity of the beam considered in this study.
4. The removal of shear links was found to decrease the shear capacity of the beam only marginally, due to the low amount of shear links and the contribution of CFRP strengthening provided.
5. Reductions in the amount of tension reinforcement were found to exert detrimental effects on the post-cracking stiffness and shear capacity. Although the amount of CFRP U-wraps considered in this study was found inadequate to recover this loss of performance, improvements in the post-peak ductility were obtained (hence decreasing the brittleness). A progressive change in failure mode toward flexure was also evident, due to reductions in flexural capacity resulting from bar reductions.
6. A similar trend of initial and post-cracking stiffnesses was observed in geometrically similar beams strengthened with three different types of FRP fabrics. The use of FRP U-wraps with relatively low stiffness (such as PET) was found to outperform the CFRP U-wraps used in the original beam.

Acknowledgements

The authors wish to acknowledge the support of both institutions and for placing the facilities of both institutions at their disposal. This paper was part of a thesis submission by the first and third authors.

References

1. Kalfat, R. and R. Al-Mahaidi, Numerical and Experimental Validation of FRP Patch Anchors

- used to Improve the Performance of FRP Laminates Bonded to Concrete, *Journal of Composites for Construction*, 18(3), 2014, p. A4013008.
2. Foster, R. M., Brindley, M., Lees, J. M., Ibell, T. J., Morley, C. T., Darby, A. P., and Evernden, M. C., Experimental Investigation of Reinforced Concrete T-Beams Strengthened in Shear with Externally Bonded CFRP Sheets, *Journal of Composites for Construction*, 21(2), 2017, pp. 1-13.
3. Mai, A.D., Sheikh, M.N., Yamakado, K., and Hadi, M.N.S., Nonuniform CFRP Wrapping to Prevent Sudden Failure of FRP Confined Square RC Columns, *Journal of Composite for Construction*, 24(6), 2020, p. 04020063.
4. Ke, Y., Zhang, S.S., Smith, S.T., and Yu, T., Novel Embedded FRP Anchor for RC Beams Strengthened in Flexure with NSM Bars: Concept and Behavior, *Journal of Composite for Construction*, 27(1), 2020, p. 04022093.
5. Valerio, P., Ibell, T.J., and Darby, A.P., Deep Embedment of FRP for Concrete Shear Strengthening, *Proceedings of the Institution of Civil Engineers-Structures and Buildings*, 162(5), 2009, pp. 311-321.
6. Tran, C.T.N., Nguyen, X.H., Nguyen, H.C., and Le, D.D., Shear Performance of Short-span FRP-reinforced Concrete Beams Strengthened with CFRP and TRC, *Engineering Structures*, 242, 2021, p.112548.
7. Tatar, J., Viniarski, C., Ishfaq, M., Harries, K.A., and Head, M., Effect of U-Wrap Anchors on Flexural Behavior of Reinforced Concrete Beams Flexurally Strengthened with Externally Bonded CFRP Sheets, *Journal of Composites for Construction*, 27(1), 2023, p. 04022099.
8. Červenka, J. and Papanikolaou, V.K., Three Dimensional Combined Fracture-Plastic Material Model for Concrete, *International Journal of Plasticity*, 24(12), 2008, pp. 2192-2220.
9. Červenka, J., Červenka, V., and Laserna, S., On Crack Band Model in Finite Element Analysis of Concrete Fracture in Engineering Practice, *Engineering Fracture Mechanics*, 197, 2018, pp. 27-47.
10. Vecchio, F.J., Disturbed Stress Field Model for Reinforced Concrete: Formulation, *Journal of Structural Engineering*, 126(9), 2000, pp. 170-177.
11. Tambusay, A., Suprobo, P., Suryanto, B., and Don, W., Application of Nonlinear Finite Element Analysis on Shear-Critical Reinforced Concrete Beams, *Journal of Engineering and Technological Sciences*, 53(4), 2021, pp. 210408.
12. Don, W., Suryanto, B., Tambusay, A., and Suprobo, P., Forensic Assessments of the Influence of Reinforcement Detailing in Reinforced Concrete Half-Joints: A Nonlinear Finite Element Study, *Structures*, 38, 2022, pp. 689-703.

13. Červenka, V., Jendele, L., and Červenka, J., ATENA Program Documentation—Part 1: Theory, *Červenka Consulting*, Prague, 2018.
14. Brindley, M., Shear Assessment and Strengthening of Reinforced Concrete T-beams with Externally Bonded CFRP Sheets, *PhD Thesis*, University of Bath, 2018.
15. BS 4449:2005+A3:2016, *Steel for the Reinforcement of Concrete – Weldable Reinforcing Steel – Bar, Coil and Decoiled Product – Specification*, British Standards Institution, 2016.
16. Menetrey, P. and Willam, K.J., Triaxial Failure Criterion for Concrete and its Generalization, *ACI Structural Journal*, 92(3), 1995, pp. 311-318.
17. Hordijk, D.A., Local Approach to Fatigue of Concrete, *PhD Thesis*, Delft University of Technology, 1991.
18. Chong, K., Suryanto, B., Tambusay, A., and Suprobo, P., Nonlinear Analysis of Reinforced Geopolymer Concrete Beams, *Civil Engineering Dimension*, 24(1), 2022, pp. 1-10.
19. Don, W., Chong, K., Aitken, M., Tambusay, A., Suryanto, B., and Suprobo, P., Influence of Link Spacing on Concrete Shear Capacity: Experimental Investigations and Finite Element Studies, *IOP Conference Series: Materials Science and Engineering*, 930(1), 2020, p. 012052.
20. Kolmar, W., Beschreibung der Kraftuebertragung Über Risse in Nichtlinearen Finite-Element-Berechnungen von Stahlbetontragwerken, *PhD Thesis*, Darmstadt University of Technology, Germany, 1986.
21. Vecchio, F.J. and Collins, M.P., The Modified Compression-Field Theory for Reinforced Concrete Elements Subjected to Shear, *ACI Journal*, 83(2), 1986, pp. 219-231.
22. Sajdlová, T., *ATENA Program Documentation Part 4-9 ATENA Science - GiD Strengthening of Concrete Structures*, Červenka Consulting, Prague, 2016.
23. Al-Saoudi, A.N., Al-Mahaidi, R., Kalfat, R., and Červenka, J., Finite Element Investigation of the Fatigue Performance of FRP Laminates Bonded to Concrete, *Composite Structures*, 208, 2019, pp. 322-337.
24. Al-Saoudi, A.N., Investigation of the Performance of Fibre Reinforced Polymers Anchorage Devices in Strengthening Concrete Bridge Beams Subjected to Fatigue Loading, *PhD Thesis*, Swinburne University of Technology, 2018.
25. Cui, S., Wang, J., Shi, L., and Liu, Y., Test and FEM Analysis of Debonding Failure of RC Beam Strengthened with CFRP, *Journal of Reinforced Plastics and Composites*, 28(17), 2009, pp. 2151-2160.
26. Al-Saoudi, A.N., Kalfat, R., Al-Mahaidi, R., Červenka, J., and Pryl, D., Numerical and Experimental Investigation into the Fatigue Life of FRP Bonded to Concrete and Anchored with Bidirectional Fabric Patches, *Engineering Structures*, 239, 2021, p. 112335.
27. Brena, S.F., Bramblett, R.M., Wood, S.L., and Kreger, M.E., Increasing Flexural Capacity of Reinforced Concrete Beams using Carbon Fiber-Reinforced Polymer Composites, *ACI Structural Journal*, 100(1), 2003, pp. 36-46.
28. Pham, H.B. and Al-Mahaidi, R., Prediction Models for Debonding Failure Loads of Carbon Fiber Reinforced Polymer Retrofitted Reinforced Concrete Beams, *Journal of Composites for Construction*, 10(1), 2006, pp. 48-59.
29. Freddi, F. and Savoia, M., Analysis of FRP-Concrete Debonding via Boundary Integral Equations, *Engineering Fracture Mechanics*, 75(6), 2008, pp. 1666-1683.
30. Wu, Y.F., Wang, Z., Liu, K., He, W., and Wang, Z., Numerical Analyses of Hybrid-Bonded FRP Strengthened Concrete Beams, *Computer-aided Civil and Infrastructure Engineering*, 24(5), 2009, pp. 371-384.
31. ACI 447.1R-18, Report on Modeling Techniques Used in Finite Element Simulations of Concrete Structures Strengthened Using Fiber-Reinforced Polymer (FRP) Materials, *American Concrete Institute*, 2018.
32. Lu, X.Z., Teng, J.G., Ye, L.P., and Jiang, J.J., Bond-Slip Models for FRP Sheets/Plates Bonded to Concrete, *Engineering Structures*, 27(6), 2005, pp. 920-937.
33. Yao, J., Teng, J.G., and Chen, J.F., Experimental Study on FRP-to-Concrete Bonded Joints, *Composites Part B: Engineering*, 36(2), 2005, pp 99-113.
34. Wang, J., Cohesive Zone Model of Intermediate Crack-Induced Debonding of FRP-Plated Concrete Beam, *International Journal of Solids and Structures*, 43(21), 2006, pp. 6630-6648.